Computational Study of the Reaction of Atomic Oxygen with Acetone in the Gas Phase

Hua Hou, Yuzhen Li, and Baoshan Wang*

College of Chemistry and Molecular Sciences, Wuhan University, Wuhan, 430072, People's Republic of China

Received: August 18, 2006; In Final Form: September 17, 2006

Mechanisms and kinetics of the reaction of atomic oxygen with acetone have been investigated using ab initio quantum chemistry methods and transition state theory. The structures of the stationary points along the possible reaction pathways were obtained using the second-order Møller−Plesset theory and the coupled-cluster theory with single and double excitations with the triple-ζ quality basis sets. The energetics of the reaction pathways were calculated at the reduced second-order Gaussian-3 level and the extrapolated full coupled-cluster/complete basis set limit. The rate coefficients were calculated in the temperature range 200−3000 K, with the detailed consideration of the hindered internal rotation and the tunneling effect using Eckart and the semiclassical WKB approximations. It is shown that the predominant mechanism is the direct hydrogen abstraction producing hydroxyl and acetonyl radicals. Although the nucleophilic OC addition/elimination channel leading to CH_3 and CO_2 involves comparable barrier with the direct hydrogen abstraction channel, kinetically it cannot play any role in the overall reaction. It is predicted that the rate coefficients show positive temperature dependence in the range 200−3000 K and strong non-Arrhenius behavior. The tunneling effect plays a significant role. Moreover, the reaction has strong kinetic isotope effect. The calculated results are in good agreement with the available experimental data. The present rigorous theoretical work is helpful for the understanding of the characteristics of the reaction of atomic oxygen with acetone.

I. Introduction

Acetone (CH_3COCH_3) is the simplest ketone. It is one of the volatile organic compounds (VOCs) emitted into the atmosphere from a variety of anthropogenic and natural sources. Moreover, it is a potential fuel additive. The reactions between acetone and various free radicals (e.g., OH, H, O, F, Cl, etc.) play important roles in both atmospheric chemistry and combustion. While the reaction of acetone with OH radical has been well-established experimentally and theoretically,[1] the reaction between atomic oxygen, $O(^3P)$, and acetone is still not well characterized. Herein the mechanism and kinetics of the title reaction are investigated computationally using high-level ab initio quantum chemistry methods.

Acetone chemistry is also important in the surface chemical activation. Acetone possesses two chemically different sites for potential activation by atomic oxygen: an electron-deficient carbonyl carbon and six equivalent acidic methyl C−H bonds. Therefore, competitive nucleophilicity and basicity reactivity of acetone with oxygen atom can take place. For example, the reactivity of acetone on the oxygen-activated metal (e.g., silver) and metal oxide (e.g., TiO_2) surfaces has been studied considerably.[2,3] The understanding of the gaseous reactivity of acetone with $O(^3P)$ may gain new insight into such interesting phenomena for the purpose of comparison.

As summarized in Table 1, all the experimental measurements of the rate coefficient were performed three decades ago,[4−11] and the rate coefficient data are scattered below 1000 K. It appears that the reaction of $O(^3P)$ with acetone is fairly slow. The room-temperature rate coefficient is about 10^{-15} cm^3 $molecule^{-1}$ s^{-1}, which is almost 2 orders of magnitude slower than that for the OH + CH_3COCH_3 reaction. Moreover, the rate coefficients are strongly temperature-dependent. No pressure dependence has ever been observed experimentally.

TABLE 1: Rate Coefficients for the $O(^3P)$ + CH_3COCH_3 Reaction

temp (K)	k (cm^3 $molecule^{-1}$ s^{-1})	methods	ref
873	1.44×10^{-13}	thermal	4
298−621	$7.08 \times 10^{-13}e^{-2863/T}$	flow-tube/ mass spectroscopy	5
298−478	$3.16 \times 10^{-12}e^{-2536/T}$	fast-flow/ mass spectroscopy	6
298	1.13×10^{-15}	mass spectroscopy	7
300−400	$5.81 \times 10^{-12}e^{-3310/T}$	flow-tube/ mass spectroscopy	8
301−565	$1.06 \times 10^{-12}e^{-2100/T}$	discharge-flow/ chemiluminescence	9
298	1.35×10^{-15}	"homogeneous" reactor/ chemiluminescence	10
300−700	$1.66 \times 10^{-11}e^{-3000/T}$	extensive literature review	11
200−3000	$4.66 \times 10^{-23}T^{3.71}e^{-1289/T}$	best fit to the calculated rate coefficients	this work

The mechanism of the $O(^3P)$ + CH_3COCH_3 reaction was studied by Lee and Timmons in 1977 through measuring the primary H/D kinetic isotope effect.[6] It was concluded that the major reaction channel involves H atom abstraction, namely

$$O(^3P) + CH_3COCH_3 \rightarrow OH + CH_3COCH_2 \qquad (A)$$

Unfortunately, neither OH radical nor CH_3COCH_2 radical has been observed directly because of the interference of the unavoidable secondary reactions, for example

$$OH + CH_3COCH_3 \rightarrow H_2O + CH_3COCH_2 \qquad (B)$$

In this work, the structures of the stationary points on the potential energy surface for the $O(^3P)$ + CH_3COCH_3 reaction

* To whom correspondence should be addressed. Email: wangb@chem.whu.edu.cn.

10.1021/jp065346w CCC: $33.50 © 2006 American Chemical Society
Published on Web 11/17/2006

are located, and the energetics of the reaction pathway are calculated using the high-level ab initio methods. The detailed reaction mechanism is revealed, namely

$$\begin{aligned} O(^3P) + CH_3COCH_3\,(X^1A) &\rightarrow OH(X^2\Pi) + CH_3COCH_2(X^2A'') \\ &\rightarrow CH_3(X^2A_2'') + CH_3CO_2(X^2A) \rightarrow \\ &\qquad 2CH_3(X^2A_2'') + CO_2(X^1\Sigma_g^{+}) \\ &\rightarrow CH_3O(X^2A') + CH_3CO(X^2A') \\ &\rightarrow CH_3(X^2A_2'') + CH_2COOH(X^2A'') \\ &\rightarrow CH_2(X^3B_1) + CH_3COOH(X^1A') \end{aligned}$$

Note that the triplet−singlet intersystem crossing is not considered in this work. The rate coefficients and the kinetic isotope effect for the abstraction and the addition/elimination channels are calculated using transition state theory. The contributions from the tunneling effect and the hindered internal rotations are considered elaborately. Excellent agreement between experiment and theory is obtained. It is noted that the kinetic isotope effect in the range $T = 298-614$ K for the hydrogen abstraction reaction has been studied theoretically by Pudzianowski and Loew in 1983.[12] The semiempirical UHF-MNDO method[13] was used to optimize the geometry of the transition state. No energetic data were reported. The tunneling effect was calculated using the Wigner method.[14]

II. Computational Methods

1. Ab Initio Calculations. According to the spin conservation, the $O(^3P) + CH_3COCH_3$ reaction occurs on the triplet potential energy surface. Therefore, only the triplet stationary points were explored in this work. The *ab initio* calculations were carried out using the Gaussian03 suite of programs.[15] Initially, the geometries were optimized at the second-order Møller−Plesset (MP2) level[16] using analytic gradients with only valence orbitals active. The basis set used in the MP2 calculations was the standard triple-ζ 6-311G(d,p). The stationary point was characterized as a minimum (all real frequencies) or a transition state (one imaginary frequency) by determination of harmonic vibrational frequencies using analytic second derivatives at the MP2/6-311G(d,p) level of theory. The zero-point energy (ZPE) was calculated using the harmonic frequencies and scaled by a factor of 0.95.[17] Moreover, to confirm the transition states connecting the desired reactants and products, minimum energy paths (MEPs) were calculated by performing intrinsic reaction coordinates (IRC)[18] analysis at the MP2/6-311G(d,p) level of theory in both the forward and backward directions.

To check the influence of basis set and higher-level electron correlation on the MP2/6-311G(d,p) optimized geometrical parameters, further optimizations were performed using two alternative methods. One is MP2 theory but with a more flexible basis set, namely, g3mp2large,[19] which corresponds to 6-311++G(2df,2p) for the [H,C,O]-containing system of our interest. The other is coupled cluster theory with single and double excitations (CCSD)[20] using the 6-311G(d,p) basis set. The CCSD/6-311G(d,p) optimizations are very time-consuming so that only the species involved in the most important pathways were considered.

The reduced second-order Gaussian-3 theory (G3MP2)[19] was employed to obtain more reliable relative energies. The G3MP2 scheme was detailed elsewhere[19] and only a brief description is given here. Single-point energy calculations were performed at the QCISD(T)/6-31G(d) (E_1), MP2/6-31G(d) (E_2), and MP2/g3mp2large (E_3) levels of theory, respectively. The combination of these three energies gives an approximation to the total energy at the QCISD(T)/g3mp2large level. The high-level correction (HLC) takes into account the remaining deficiencies in the above energy calculations. The ΔE_{HLC} (in mhartrees) is $-4.471\ n_\alpha - 4.808\ n_\beta$ for molecules and $-2.021\ n_\alpha - 7.324\ n_\beta$ for atoms. The n_α and n_β are the number of α and β valence electrons, respectively, with $n_\alpha \geq n_\beta$. The spin-orbital correction (ΔE_{SO}) was made for atomic species. Finally the G3MP2 total energy was calculated as follows

$$E_0\,(\mathrm{G3MP2}) = E_1 + (E_3 - E_2) + \Delta E_{HLC} + \Delta E_{SO} + \mathrm{ZPE} \quad (1)$$

All HF and post-HF calculations were performed using the unrestricted methodology for both open-shell and closed-shell species. In addition, rather than the regular MP2, the spin-projected Møller−Plesset theory through the second order (PMP2)[21] was used in the calculations of E_2 and E_3 to annihilate spin contamination. However, this alternation does not have significant impact on the calculated relative energies.

The G3MP2 theory has been widely used in the calculation of both barrier height and heat of reaction for many chemical reactions because of its efficiency. However, it is an empirical composite method and has not been designated for the characterization of the saddle point. Therefore, for the most important reaction pathways the energies at the CCSD/6-311G(d,p) optimized geometries were corrected for basis set and CI truncated errors using the extrapolated full coupled cluster/complete basis set method (FCC/CBS). The basis set error was corrected using the following formula[22,23]

$$\begin{aligned} E_{HF}(X) &\approx E_{HF}(\infty) + a\mathrm{e}^{-bX} \\ \Delta E^{corr}_{CCSD(T)}(X) &\approx \Delta E^{corr}_{CCSD(T)}(\infty) + c(X + 0.5)^{-3} \end{aligned} \quad (2)$$

where $E_{HF}(X)$ and $E_{HF}(\infty)$ are the HF energies calculated with the basis set cc-pVXZ (X represents the cardinal number 2, 3, 4 for VDZ, VTZ, VQZ) and at the complete basis set (CBS) limit, respectively. $\Delta E^{corr}_{CCSD(T)}(X)$ and $\Delta E^{corr}_{CCSD(T)}(\infty)$ are the correlation energies calculated at the CCSD(T) level with the basis set cc-pVXZ ($X = 2$ and 3) and at the CBS limit, respectively, and a, b, and c are the parameters to be determined. The CI truncated error was estimated using the perturbational energy of the connected triple excitations calculated at the CCSD(T)/cc-pVTZ level ($E^{T}_{CCSD(T)/cc-pVTZ}$). Because the perturbational energy of the connected triple excitation accounts for only about 80% of the full triple- and higher-order contributions,[24] the CI truncated error was approximated to be $^1/_5 E^{T}_{CCSD(T)/cc-pVTZ}$. The FCC/CBS energy can be then written as follows

$$\begin{aligned} E_{FCC/CBS} = E_{HF}(\infty) + \Delta E^{corr}_{CCSD(T)/cc-pVTZ} + (125/218) \times \\ [\Delta E^{corr}_{CCSD(T)/cc-pVTZ} - \Delta E^{corr}_{CCSD(T)/cc-pVDZ}] + \\ {}^1/_5 E^{T}_{CCSD(T)/cc-pVTZ} \end{aligned} \quad (3)$$

It is noted that the unrestricted HF reference wave function was used in all the coupled cluster energy calculations.

2. Kinetic Calculations. The temperature-dependent rate coefficients were calculated using the conventional transition state theory, namely

$$k(T) = l \cdot \kappa \cdot \frac{k_B T}{h} \cdot \frac{Q^{\neq}}{Q_O Q_{acetone}} e^{-E^{\neq}_0/RT} \quad (4)$$

where l is the statistical factor (or the reaction path degeneracy); κ is the tunneling transmission coefficient; k_B is the Boltzmann constant; h is the Planck constant; $Q^{\neq}$, Q_O, and $Q_{acetone}$ are the partition functions of the transition state, the reactants O(^{3}P), and acetone, respectively; $E^{\neq}_0$ is the barrier height at 0 K obtained directly from the ab initio calculations; R is the ideal gas constant; and T is the temperature.

The partition function was calculated using the standard statistical mechanics, namely

$$Q = Q_e\, Q_t\, Q_r\, Q_v\, Q_{int} \quad (5)$$

While the electronic (Q_e), translational (Q_t), rotational (Q_r), and vibrational (Q_v) partition functions have the respective standard formula, the treatment of the internal rotational degrees of freedom (Q_{int}) is much more complicated. In this work, the possible internal rotations in the reactant (acetone) and the transition states have been identified using the methods of Ayala and Schlegel.[25] All internal rotors were treated using the multidimensional hindered rotation model, and the partition function Q_{int} was calculated using the best-fit expressions in ref 25.

Two methods were employed to estimate the tunneling factor κ. One is the Eckart formula, which is determined only by the imaginary frequency of the transition state ($\nu^{\neq}$), the barrier height ($E^{\neq}_0$), and the heat of reaction at 0 K ($\Delta_r H^0$).[26] The other is the semiclassical WKB approximation with the dual-level interpolations MEP potential, namely[27,28]

$$\kappa = 1 + \frac{2}{k_B T}\int_{E_0}^{E^{\neq}_0} P(E) \sin h\,[(E^{\neq}_0 - E)/k_B T]\, dE \quad (6)$$

where $E_0 = [\max(0, \Delta_r H^0)]$ and $E^{\neq}_0$ are the threshold energy and the barrier height, respectively. $P(E)$ is the transmission probability through a one-dimension barrier at energy E, $E_0 \le E \le E^{\neq}_0$, namely[27]

$$P(E) = \frac{1}{1 + e^{2\theta(E)}}, \quad \theta(E) = \frac{2\pi}{h}\int_{s_1}^{s_2} \sqrt{2\mu_{eff}(s)|E - V^G_a(s)|}\, ds \quad (7)$$

where s is the reaction coordinate originated at the saddle point; s_1 and s_2 are the classical turning points, that is, the location where $V^G_a(s) = E$; $V^G_a(s)$ is the vibrational adiabatic ground state potential, which is approximated to be $V^G_a(s) = V_{MEP}(s) + V_{ZPE}(s)$. $V_{MEP}(s)$ and $V_{ZPE}(s)$ are the potential along the MEP obtained from the IRC calculation and the vibrational zero-point energy along the MEP, respectively. In the mass-weighted Cartesian coordinate system and with the assumption of the zero-curvature tunneling, the effective reduced mass of the system $\mu_{eff}(s)$ is equal to 1. It is noted that the nonclassical reflection above threshold has been included in the eq 6 implicitly by the definition of $P(E)$ as follows[27]

$$\begin{aligned} P(E) &= 1 - P(2E^{\neq}_0 - E), \quad E^{\neq}_0 \le E \le 2E^{\neq}_0 - E_0 \\ P(E) &= 1, \quad 2E^{\neq}_0 - E_0 < E \end{aligned} \quad (8)$$

The key point to calculate κ is to use a realistic $V^G_a(s)$. However, because of the technical difficulties, $V_{MEP}(s)$ and $V_{ZPE}(s)$ can be calculated only at some low levels of theory such as MP2/6-311G(d,p) in this work. To obtain a better $V^G_a(s)$, a dual-level method[28] was used in which the low level $V_{MEP}(s)$ was corrected by interpolating the energy difference at the saddle points between low-level calculations [e.g., MP2/6-311G(d,p)] and high-level single-point energy calculation (e.g., FCC/CBS). The MEPs for H-abstraction and addition/elimination pathways were calculated in the mass-weighted Cartesian coordinate system with the stepsize of 0.01 amu$^{1/2}$ bohr from the saddle points to both reactant and product sides (ca. 500−600 points for each pathway). $V_{ZPE}(s)$ was not calculated using ab initio methods because it is too time-consuming. Alternatively, the value of $V_{ZPE}(s)$ at the specific s was obtained through the spline interpolation of the zero-point energies of the reactant, the saddle point, and the products along the MEPs.

All the input data for the kinetic calculations can be obtained from the ab initio calculations using the Gaussian03 program. It is noted that the symmetry numbers are excluded in the calculations of the rotational partition functions Q_r since the explicit statistical factors (e.g., $l = 6$ for H-abstraction and $l = 2$ for addition/elimination pathways) were used.

III. Results and Discussion

The calculated energetic reaction pathways are shown in Figure 1. The structures of the stationary points (intermediates and transition states) are shown in Figures 2 and 3. The corresponding energies of all the reaction pathways calculated at various levels of theory are summarized in Table 2. It is noted that the theoretical heats of reaction at 298.15 K ($\Delta_r H^{298}$) for the five product channels are in reasonable agreement with the experimental data.[29] The rate coefficients in the temperature range of 200−3000 K are shown in Figure 4. The calculated kinetic isotope effect [e.g., the O(^{3}P) + CH_3COCH_3 reaction versus the O(^{3}P) + CD_3COCD_3 reaction] is shown in Figure 5.

1. Reaction Mechanisms. Four types of possible reaction pathways between O(^{3}P) and acetone have been explored, including the direct hydrogen abstraction from one of the methyl groups of acetone, the nucleophilic addition toward the electron-deficient carbonyl carbon of acetone and the subsequent decomposition and isomerization of the adduct, the addition toward the carbonyl oxygen of acetone, and the S_N2-type displacement reaction. These reaction mechanisms will be discussed separately as follows in terms of their structural and energetic characteristics.

A. Direct H-Abstraction Reaction. The reaction of O(^{3}P) with acetone takes place through the long-range interaction between O(^{3}P) and the two relatively large methyl groups of acetone. A weakly bonded complex, HBC1, exists between O(^{3}P) atom and the two equivalent acidic methyl CH bonds. The two O···H distances are longer than 3 Å. As shown in Table 1, the interaction energy is only 0.4 kcal/mol at the FCC/CBS level and, apparently, it is overestimated by the empirical G3MP2 theory.

The transition state for the H-abstraction is labeled as TS1, as shown in Figure 2. TS1 has no symmetry, even though the reactant acetone is symmetric and the six C−H bonds are nearly equivalent. When the structural parameters obtained at three levels of theory, namely, MP2/6-311G(d,p), MP2/g3mp2large, and CCSD/6-311G(d,p), are compared one to another, it is found that they are consistent with each other. The breaking CH bond and the forming HO bond are 1.3 and 1.2 Å, respectively. The reacting O−H−C geometry deviates from linearity slightly by about 3−7 degrees. The remaining geometrical parameters are very similar to those of acetone. In the previous UHF-MNDO study,[12] the CH and OH distances were reported to be 1.237 and 1.308 Å, respectively, with a linear O−H−C geometry.

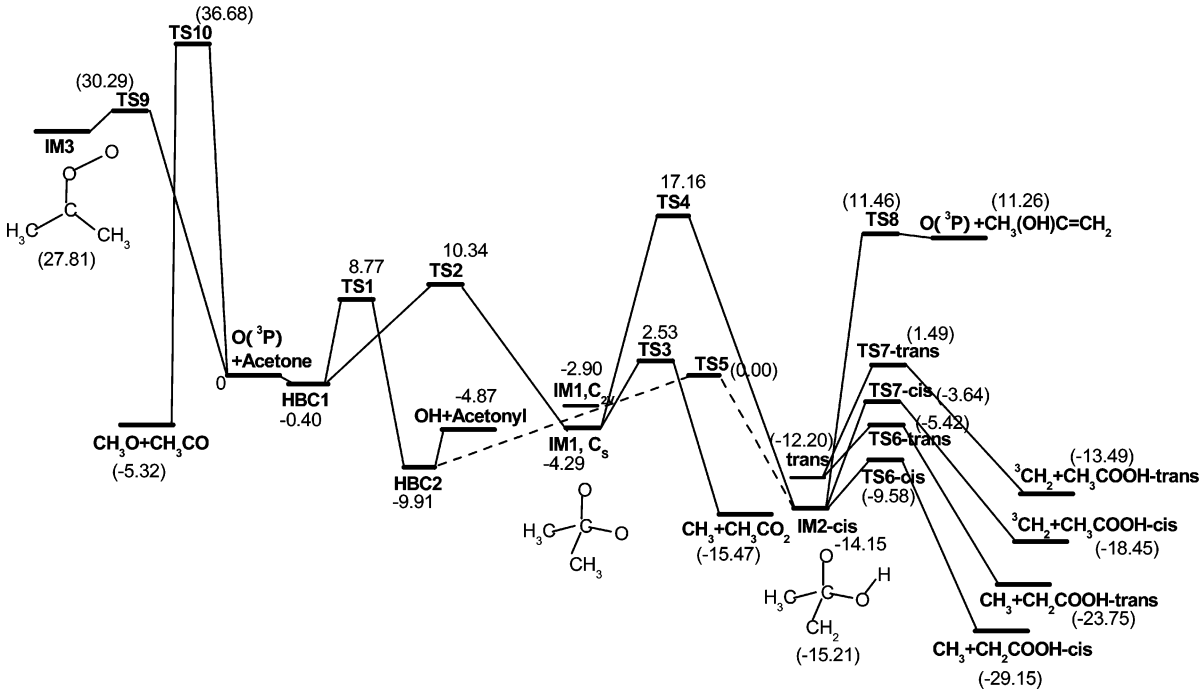

Figure 1. Energetics of the reaction pathways for the reaction of O(^{3}P) with acetone. The energies calculated at the FCC/CBS//CCSD/6-311G(d,p) level are shown in kcal/mol. The energies in parenthesis correspond to the G3MP2//MP2/6-311G(d,p) level.

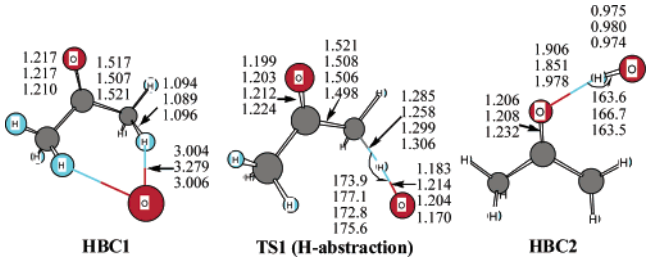

Figure 2. Geometries of the stationary points involved in the direct hydrogen abstraction mechanism for the O(^{3}P) + CH_3COCH_3 reaction. Bond distances are in angstroms and bond angles are in degrees. From top to bottom, the three entries correspond to the geometrical parameters optimized at the MP2/6-311G(d,p), MP2/g3mp2large, and CCSD/6-311G(d,p) levels of theory, respectively. For TS1, the fourth entries represent the optimized parameters at the CAS(10,8)/6-311G(d,p) level.

Evidently, the semiempirical MNDO method gives a more reactant-like transition state for the abstraction contrary to the present higher-level ab initio results. The ZPE-corrected barrier height was calculated to be 8.77 kcal/mol at the FCC/CBS level. As shown in Table 1, the G3MP2 calculated barrier heights at three optimized geometries are in good agreement with the FCC/CBS value especially the G3MP2//MP2/6-311G(d,p) level of theory. This implies that the computationally most efficient G3MP2//MP2/6-311G(d,p) method might be good enough at least qualitatively to characterize the potential energy surface.

The hydrogen abstraction produces hydroxyl and acetonyl radicals with an exothermicity of about 5 kcal/mol. Theoretically, a hydrogen-bonding complex (HBC2) can be formed between the two product molecules, as shown in Figure 2. The hydrogen bonding occurs between the H atom of OH and the O atom of CH_3COCH_2, and the hydrogen-bond distance is nearly 2 Å. The binding energy of HBC2 is about 5 kcal/mol at 0 K.

B. OC Addition/Elimination Mechanism. The OC addition between O(^{3}P) and acetone takes place via transition state TS2. As shown in Figure 3, TS2 has C_s symmetry and ^{3}A″ electronic state. The optimizations at the MP2 level with either 6-311G-(d,p) or g3mp2large basis set gave similar geometrical parameters, whereas the CCSD/6-311G(d,p) level predicts slightly longer CO bonds and a larger OCO bond angle. The forming CO bond is nearly 1.8 Å. The original C═O double bond in acetone changes to single bond by elongating the distance from 1.21 Å to 1.26 Å. The ZPE-corrected barrier height for TS2 is 10.34 kcal/mol at the FCC/CBS level. The G3MP2 calculated barrier heights at the three optimized geometries are about 1.5 kcal/mol lower, but they are still in the range of the uncertainty of the G3MP2 calculated energies.[19]

It is worthy of comparing the barrier heights for TS1 and TS2 because they are the most important stationary points along the reaction pathways. Apparently TS1 is lower than TS2. However, interestingly, without ZPE corrections, the energy of TS1 is even higher than that of TS2. At the FCC/CBS level of theory, the classical barrier heights (e.g., excluding ZPE) for TS1 and TS2 are 11.41 and 9.59 kcal/mol, respectively. Evidently, TS1 is almost 2 kcal/mol higher than TS2. Therefore, the ZPE has a significant effect on the barrier heights. As can be drawn from Table 2, with respect to the O(^{3}P) + CH_3COCH_3 reactants, the ZPE contribution to the barrier height for TS1 is −2.64 kcal/mol, while that for TS2 is +0.75 kcal/mol at the MP2/6-311G(d,p) level. Moreover, ZPEs were calculated at the CCSD/6-311G(d,p) level. The ZPE contribution to the barrier height for TS1 is −3.46 kcal/mol, while that for TS2 is +0.45 kcal/mol, corresponding to the ZPE-corrected barrier heights for TS1 and TS2 to be 7.95 and 10.04 kcal/mol, respectively. The results are in agreement with those obtained at the MP2/6-311G(d,p) level.

The OC addition leads to the adduct $(CH_3)_2CO_2$ (denoted as IM1), which is a biradical species. Interestingly, there are two conformers of IM1 with different symmetries. One has C_s symmetry with the OCO symmetrical plane and ^{3}A″ electronic state. The two CO bond distances are slightly different. The other conformer has C_{2V} symmetry with the OCO and CCC symmetrical planes and a C_2 axis and ^{3}A$_2$ electronic state. The two equivalent CO bond distances are shorter than either of the CO bonds of the C_s structure. In terms of energy, the C_s

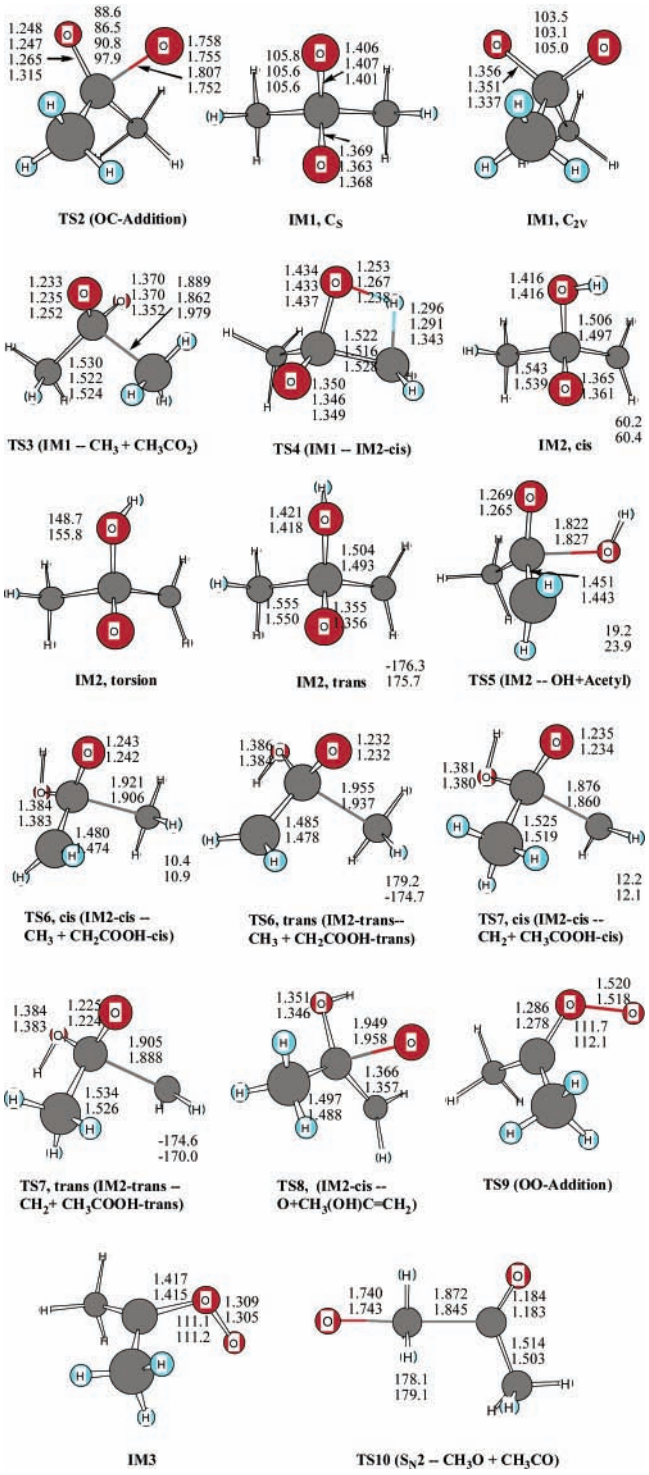

Figure 3. Geometries of the stationary points involved in the addition/elimination and S_N2-type displacement mechanisms for the $O(^3P)$ + CH_3COCH_3 reaction. Bond distances are in angstroms and bond angles are in degrees. From top to bottom, the entries correspond to the geometrical parameters optimized at the MP2/6-311G(d,p), MP2/g3mp2large, and CCSD/6-311G(d,p) levels of theory, respectively. For TS2, the fourth entries represent the optimized parameters at the CAS-(10,8)/6-311G(d,p) level.

structure is more stable than the C_{2v} structure. The reason for the existence of two such structures can be understood in view of their electron configurations, as shown in Scheme 1. Clearly, the relative orientation of the lone-pair electrons in O atoms determines the symmetry of IM1. For the C_{2v} structure, because

SCHEME 1

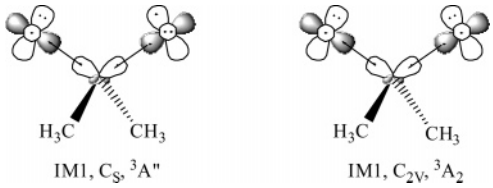

of the stronger repulsion between the two in-plane lone-pair electrons, its energy is slightly higher than that of the C_s structure.

The IM1 adduct is not an energy-rich intermediate because its energy is only about 4 kcal/mol lower than that of the $O(^3P)$ + CH_3COCH_3 reactants. This energy is even less than the heat released in the abstraction product channel. However, there is a product channel with a small amount of barrier, that is, the transition state TS3 for the elimination of CH_3 to form CH_3-CO_2 radical. At the FCC/CBS level of theory, the barrier height is 2.53 kcal/mol with respect to the initial $O(^3P)$ + CH_3COCH_3 reactants. The production of CH_3 + CH_3CO_2 is exothermic by 15.47 kcal/mol. It is noted that the product CH_3CO_2 is unstable. The barrier height for the secondary decomposition, CH_3CO_2 → CH_3 + CO_2, is only about 4 kcal/mol.[30] Therefore, the reaction energy may drive it to decompose further to form CH_3 and CO_2. Comparing the geometries of TS3 and IM1, it is shown that the breaking CC bond is stretched by about 20% and, simultaneously, one of the CO bonds is shortened by about 10% while the other CO bond remains unchanged.

The other possible reaction starting from IM1 is the isomerization to form another intermediate (IM2) via a four-center transition state TS4. One of the hydrogen atoms of the CH_3 group is shifted to one of the O atoms. The barrier height for TS4 is as high as 17.16 kcal/mol at the FCC/CBS level. The G3MP2 method gives a similar barrier height. Evidently, this isomerization pathway is unimportant and it should not play any role in the overall reaction. The formation of IM2 is exothermic by about 15 kcal/mol. A few product channels for the subsequent decomposition of IM2 exist. For example, the C−OH bond cleavage forms OH + CH_3COCH_2 via transition state TS5. The energy of TS5 was calculated to be nearly equal to that of the $O(^3P)$ + CH_3COCH_3 reactants. In addition, the C−CH_3 bond fission leads to CH_3 and CH_2COOH via transition state TS6; the C−CH_2 bond fission leads to $CH_2(X^3B_2)$ and CH_3COOH via transition state TS7. Both TS6 and TS7 are relatively low barriers. It is worth noting that the above reaction pathways starting from IM2 have the typical anisotropic feature, that is, there are two different conformations (*cis* and *trans*), depending on the HOCO dihedral angle. The *cis*-conformers have lower energies. The *trans*-conformers lie about 3−5 kcal/mol above the *cis*-conformers. Note that TS5 is an exception and only the *cis*-conformer exists. The last reaction pathway for IM2 is the C−O bond fission leading to atomic oxygen and $CH_3C(OH)$=CH_2, which is an isomer of acetone. This channel is endothermic and, thus, is negligible.

C. OO Addition Reaction. The OO addition reaction takes place via transition state TS9. As shown in Figure 3, the forming OO bond is 1.52 Å and the original C=O double bond is elongated to 1.286 Å. The barrier for TS9 is more than 30 kcal/mol high, which is about 20 kcal/mol higher than the barrier for the OC addition reaction. Therefore, the OO addition is negligible. Moreover, the adduct IM3 is also a biradical and its energy is well above that of the reactants. No further study on this channel was performed.

TABLE 2: Relative Energies (in kcal/mol) of Various Species Involved in the Reaction of $O(^3P)$ with CH_3COCH_3

species	$\langle S^2\rangle^a$	ZPE[b]	G3MP2//MP2/6-311G(d,p)[c]	G3MP2//MP2/g3mp2large	G3(MP2)//CCSD/6-311G(d,p)	FCC/CBS//CCSD/6-311G(d,p)	$\Delta_r H^{298d}$
$O(^3P)$ + acetone	2.005, 0	50.41 (50.38)	0	0	0	0	
HBC1, $OC(CH_3)_2\cdots O$	2.006	50.53	−3.58	−4.21	−3.57	−0.4	
TS1	2.080	47.77 (46.92)	8.74	8.61	7.92	8.77	
HBC2, $CH_3C(CH_2)O\cdots HO$	2.091	49.84	−10.82	−10.93	−11.89	−9.91	
$OH + CH_3COCH_2$	0.755, 0.848	48.07	−5.77 (−5.16)	−5.95	−7.23	−4.87	−7.0∼−4.6
TS2, C_S ($^3A''$)	2.169	51.16 (50.83)	8.77	9.09	8.59	10.34	
IM1, $(CH_3)_2CO(O)$, C_S ($^3A''$)	2.016	52.70	−6.01	−5.98	−6.08	−4.29	
IM1, $(CH_3)_2CO(O)$, C_{2V} ($^3A_2$)	2.078	55.20	−3.25	−3.15	−3.22	−2.90	
TS3	2.099	51.02	1.75	1.79	2.79	2.53	
$CH_3 + CH_3CO_2$	0.762, 0.758	46.92	−15.47 (−14.85)	−15.51	−16.11	−13.83	−17.9
TS4	2.053	49.17	17.66	17.63	17.38	17.16	
IM2-*cis*, $CH_3CO(OH)CH_2$	2.022	51.31	−15.21	−15.24	−15.26	−14.15	
IM2-torsion	2.023	50.84	−12.16	−12.25			
IM2-*trans*, $CH_3CO(OH)CH_2$	2.024	51.00	−12.20	−12.55			
TS5 (*cis*)	2.179	49.89	0.00	0.14			
TS6 (*cis*)	2.121	49.69	−9.58	−9.42			
CH_3 + *cis*-CH_2COOH	0.762, 0.793	47.44	−29.15 (−28.70)	−29.26			−31
TS6 (*trans*)	2.137	49.46	−5.42	−5.26			
CH_3 + *trans*-CH_2COOH	0.762, 0.805	47.18	−23.75	−23.94			
TS7 (*cis*)	2.107	50.06	−3.64	−3.53			
$^3CH_2$ + *cis*-CH_3COOH	2.016, 0	47.92	−18.45 (−18.04)	−18.48			−17.4
TS7 (*trans*)	2.121	49.77	1.49	1.62			
$^3CH_2$ + *trans*-CH_3COOH	2.016, 0	47.67	−13.49	−13.52			
TS8 (*cis*)	2.199	51.54	11.46	11.92			
$O(^3P) + CH_3(OH)C{=}CH_2$	2.005, 0	50.92	11.26	11.25			
TS9	2.234	50.46	30.29	30.70			
IM3, $(CH_3)_2COO$	2.026	51.96	27.81	27.96			
TS10 (S_N2)	2.152	49.84	36.68	37.04			
$CH_3O + CH_3CO$	0.758, 0.763	48.63	−5.32 (−5.18)	-5.28			−5.7

[a] Expectation values of the UHF/6-311G(d,p) reference wave function. The exact values for doublet and triplet are 2 and 0.75, respectively. [b] At the MP2/6-311G(d,p) level of theory and scaled by 0.95. The values in parenthesis are obtained at the CCSD/6-311G(d,p) level and scaled by 0.95. [c] The values in parenthesis correspond to the relative energies at 298.15 K. [d] Experimental values taken from ref 29.

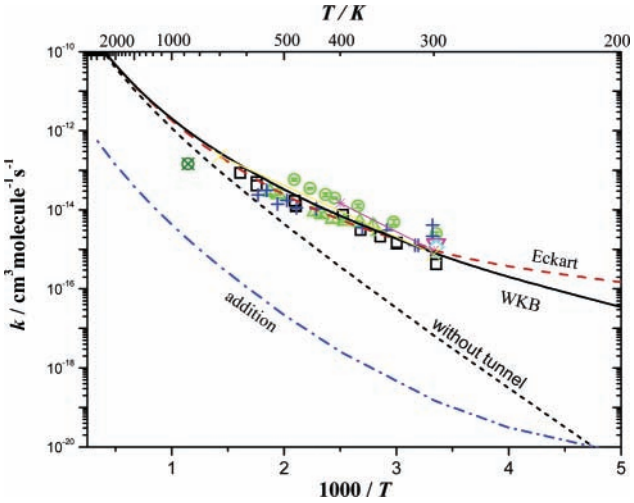

Figure 4. Logarithm plot of the rate coefficients for the $O(^3P) + CH_3COCH_3$ reaction in the temperature range 200−3000 K. The calculated rate coefficients for the hydrogen abstraction channel are shown by the solid line (with the WKB tunneling), the dashed line (with the Eckart tunneling), and the short dashed line (without tunneling), respectively. The rate coefficients for the OC-addition channel are shown by the dot-dashed line (with the WKB tunneling). The symbols show the experimental data: ⊗, ref 4; □, ref 5; △, ref 6, the MS-measured data; ○, ref 6, the ESR-measured data; ◇, ref 7; ∗—∗, ref 8; +, ref 9; ▽, ref 10; ×— ×, ref 11.

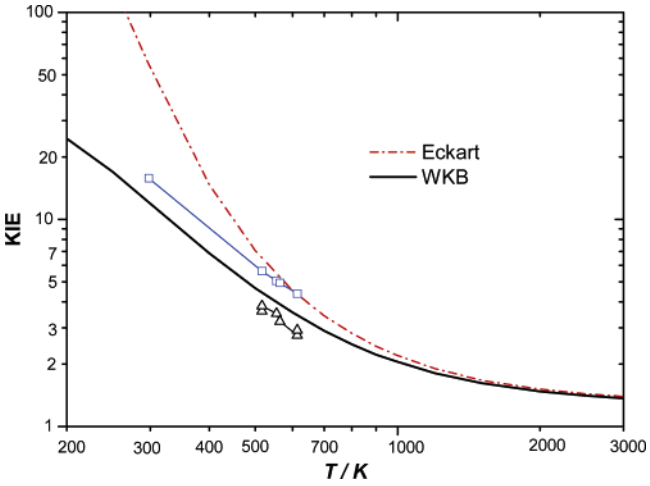

Figure 5. Kinetic isotope effect (KIE) for the $O(^3P) + CH_3COCH_3$ reaction in the temperature range 200−3000 K. The KIEs with the WKB tunneling and with the Eckart tunneling are shown by the solid line and the dot-dashed line, respectively. Δ, the experimental data in ref 6; □, the theoretical data in ref 12.

D. The S_N2-Type Displacement Reaction. The attacking of $O(^3P)$ to one of the methyl groups of acetone occurs via transition state TS10, forming CH_3O and CH_3CO radicals. Although this channel is exothermic by about 5 kcal/mol, the barrier for TS10 represents the highest barrier among the stationary points calculated in this work, as shown in Figure 1. Therefore, this displacement path is negligible.

In summary, there are two important reaction pathways in view of the theoretical barriers, namely, the direct abstraction path

$$O(^3P) + CH_3COCH_3 \rightarrow HBC1 \rightarrow TS1 \rightarrow HBC2 \rightarrow OH + CH_3COCH_2$$

and the nucleophilic OC-addition/elimination path

$$O(^3P) + CH_3COCH_3 \rightarrow HBC1 \rightarrow TS2 \rightarrow (CH_3)_2CO_2\ (IM1) \rightarrow TS3 \rightarrow CH_3 + CH_3CO_2$$

where the rate-determining step is the formation of IM1 via TS2. The other pathways are negligible because significant barriers are involved. To determine which pathway is the major reaction channel, kinetic calculations have been carried out. For simplicity, the rate coefficients of the overall reaction were calculated using only the transition states TS1 and TS2.

2. Kinetic Calculations. The essential input data for the calculations of the rate coefficients are summarized in Table 3. The MEP was calculated at the MP2/6-311G(d,p) level of theory using the IRC techniques implemented in Gaussian03 software. The step size of 0.01 amu$^{1/2}$bohr was employed for the reaction coordinate (*s*). The final MEPs for the abstraction (TS1) and the addition (TS2) consist of 533 and 600 geometries and energies, covering the reaction coordinates from −3.13 to 2.19 and from −4.0 to 2.0 amu$^{1/2}$bohr, respectively (Supporting Information, Table S1). These MEP energies were interpolated to the FCC/CBS calculated barrier heights and heats of reaction.

A. Temperature-Dependent Rate Coefficient. The rate coefficients were calculated in the temperature range of 200−3000 K. The results are shown in Figure 4 to compare with the previous experimental values. A few conclusions can be drawn from this figure.

First, the rate coefficients for the addition reaction are negligible in comparison with those for the hydrogen abstraction. Even at the highest temperature (3000 K) considered in this work, the contribution of the addition to the overall reaction is less than 1%. The higher barrier and the smaller tunneling effect for the addition reaction account for its slower rate. This result is in agreement with the experimental observation,[6] in which only the hydrogen abstraction mechanism was observed. In addition, the lack of pressure dependence of the rate coefficients implies that the addition/elimination mechanism is negligible.

Second, the calculated rate coefficients with either WKB or Eckart tunneling correction for the hydrogen abstraction are in good agreement with the experimental data. It is worth noting that there are two sets of experimental data reported by Lee and Richard.[6] One was measured using mass spectrometry (MS), and the other was measured using the electron spin resonance (ESR) technique. The authors claimed, and also confirmed later by Roscoe using the discharge-flow/chemiluminescence technique,[9] that the MS measured data are more reliable and the ESR measured data are overestimated. As can be seen in Figure 4, the present theoretical rate coefficients are in better agreement with the MS measured data. For practical use, the theoretical rate coefficients were fitted using the empirical expression as follows (in the unit of cm^{3}molecule^{-1}s^{-1})

$$k(T) = 4.66 \times 10^{-23} T^{3.71} e^{-1289/T}, \quad 200 \le T \le 3000\ K$$

Evidently, the rate coefficients show strong non-Arrhenius behavior.

Third, the tunneling effect is significantly below 1000 K for the abstraction reaction. At the lowest temperature (200 K) considered in this work, the tunneling correction factor is as large as 10^4. At room temperature, the tunneling correction factor is about 120. On the other hand, it appears that the simple Eckart formula predicts a similar tunneling effect to the complicated WKB method, although at lower temperatures the Eckart tunneling is overestimated. It should be noted that the shape of the potential V_a^G either calculated at the MP2/6-311(d,p) level or interpolated at the FCC/CBS level cannot be well approximated using the Eckart potential.

B. Kinetic Isotope Effect. The kinetic isotope effect (KIE) was calculated as the ratios of the rate coefficients for the $O(^3P) + CH_3COCH_3$ reaction with those for the $O(^3P) + CD_3COCD_3$ reaction, namely

$$KIE = k_{O+CH_3COCH_3}/k_{O+CD_3COCD_3}$$

Only the abstraction mechanism was considered in the calculation because the nucleophilic reaction path would not be expected to show an appreciable kinetic isotope effect. The KIE data in the temperature range 200−3000 K are shown in Figure 5, together with the experimental data measured by Lee and Timmons using the MS technique.[6] The temperature dependence of KIE is in excellent agreement with the experimental one. However, the theoretical KIEs are generally larger than the experimental data by about 20%. This deviation might indicate insufficient treatment of the tunneling effect using the one-dimensional models here because the real tunneling is a multidimensional problem. On the other hand, there are unknown uncertainties in the experimental data, which were claimed to be "*meaningful only from the standpoint of order of magnitude considerations and not in terms of quantitative data*."[6] In addition, the predicted KIEs with Eckart tunneling are even larger than those with the WKB tunneling, especially at intermediate temperatures and below (e.g., <500 K).

It is noted that KIEs were calculated by Pudzianowski and Loew using the UHF-MNDO theory and the Wigner tunneling correction.[12] Their data are shown in Figure 5 for comparison. While a similar trend is obtained with the present KIE data, the previous data are generally larger by about 50%. Coincidently, the MDNO KIEs are in agreement with our data using the Eckart tunneling at intermediate temperatures (ca. 500 K). At $T = 500$ K, the Wigner tunneling factor is 2.6, which is only half of the Eckart tunneling factor (5.3) or one-third of the WKB value (7.2). The lower the temperature, the larger the difference between the Wigner tunneling factors and the Eckart or WKB tunneling factors. Therefore, the apparent agreement between the previous MNDO/Wigner KIEs and the present KIEs does not mean that the reaction of $O(^3P)$ with acetone can be well described using the MNDO theory.

3. Error Analysis. Because the variational effect is not considered in the framework of the transition state theory, the theoretical rate coefficients represent an upper limit. In the theoretical viewpoint, the variational effect is presumably insignificant for the current reaction involving the relatively high barriers. It is conceivable that the neglect of the variational effect should just cause a minor error in the calculation of the rate coefficients. The other possible error lies in the treatment of the semiclassical tunneling effect. It is hard to estimate the uncertainty of the tunneling factor calculated using the one-dimensional potential models. However, as indicated by the reasonable agreement between the theoretical KIEs with the experimental data, the present tunneling corrections appear to be quantitatively reliable.

The most significant error might result from the uncertainties of the calculated barrier heights, especially for the transition states TS1 and TS2. As shown in Table 2, the expectation values of $\langle S^2 \rangle$ of the HF reference wavefunctions for TS1 and TS2 are 2.080 and 2.169, respectively, while the exact value is 2 for triplet. It has been shown that the barrier height can be overestimated or underestimated significantly due to spin contamination.[31,32] To investigate the potential multireference feature of the stationary points along the reaction path, the

TABLE 3: Input Parameters for the Transition State Theory Calculations of the Rate Coefficients for the $O(^3P) + CH_3COCH_3$ Reaction[a]

species	electronic parameters	moment of inertia (I_A, I_B, I_C)	internal rotation parameters (harmonic freq., internal rotator freq., reduced moment of inertia, symmetry number, and multiplicity)	vibrational frequencies[b]
$O(^3P)$	$5 + 3e^{-228/T} + e^{-326/T}$			
CH_3COCH_3	1	179.5, 211.3, 368,	479, 101, 1.2316, 1.0, 1.0, 139, 165, 1.1491, 1.0, 1.0	377, 481, 534, 804, 889, 906, 1091, 1121, 1254, 1395, 1406, 1482, 1486, 1492, 1507, 1788, 3075, 3080, 3158, 3163, 3204, 3205
CD_3COCD_3	1	215.1, 280.7, 451.1	56, 72, 2.4250, 1.0, 1.0, 103, 121, 2.1390, 1.0, 1.0	316, 401, 481, 672, 711, 726, 902, 982, 1026, 1068, 1070, 1076, 1085, 1116, 1280, 1779, 2210, 2213, 2336, 2341, 2376, 2378
TS1	3	265.0, 608.8, 726.5	31, 55, 7.3107, 1.0, 2.0, 129, 155, 1.2828, 1.0, 1.0	2136*i*, 129, 358, 421, 507, 530, 634, 802, 844, 887, 1071, 1116, 1197, 1214, 1265, 1399, 1453, 1486, 1496, 2357, 3085, 3140, 3173, 3218, 3250
TS1-d_6	3	330.7, 649.6, 795.6	28, 49, 8.6740, 1.0, 2.0, 88, 116, 2.5473, 1.0, 1.0	1559*i*, 116, 279, 335, 435, 473, 548, 645, 698, 710, 866, 878, 948, 998, 1033, 1067, 1079, 1114, 1275, 2215, 2272, 2346, 2348, 2391, 2418
TS2	3	339.7, 343.7, 403.9	169, 177, 1.2477, 1.0, 1.0, 224, 234, 1.2089, 1.0, 1.0	1047*i*, 243, 295, 403, 475, 514, 805, 910, 956, 1023, 1094, 1259, 1408, 1409, 1468, 1487, 1491, 1508, 1560, 3088, 3091, 3181, 3185, 3209, 3212

[a] Moments of inertia are in amu bohr^2 and frequencies are in cm^{-1}. [b] Unscaled frequencies at the MP2/6-311G(d,p) level; *i* represents imaginary frequency.

TABLE 4: Energies of the Reactants, TS1, and TS2 Calculated Using the MCSCF and MRCI Methods[a]

species	C^2_{HF}[b]	ZPE[c]	CAS(10,8)/6-311G(d,p)	MR+Q(10,8)/6-311G(d,p)	MR+Q(10,8)/6-311++G(3df,3pd)
$O+CH_3COCH_3$	0.920	50.21	−266.845 075	−267.607 972 (0)	−267.764 808 (0)
TS1	0.906	46.78	−266.816 664	−267.582 521 (12.54)	−267.745 602 (8.62)
TS2	0.895	51.27	−266.825 272	−267.587 283 (14.04)	−267.748 852 (11.07)

[a] The values in parenthesis are the relative energies (barrier heights) of TS1 and TS2 with the ZPE corrections. [b] Reference coefficients of the HF determinant. [c] Calculated at the CAS(10,8)/6-311G(d,p) level and scaled by a factor of 0.905 according to the HF/6-311G(d,p) scaling factor in ref 17.

multiconfigurational self-consistent-field (MCSCF) calculations were carried out for the supermolecule $O+CH_3COCH_3$ (e.g., O and CH_3COCH_3 are separated by 100 Å), TS1, and TS2. The active space includes ten electrons distributed in eight orbitals in the scheme of the complete active space [e.g., CAS(10,8)] procedure[33] implemented in Gaussian03. The geometries of $O+CH_3COCH_3$, TS1, and TS2 were optimized at the CAS-(10,8)/6-311G(d,p) level of theory, and the results are shown in Figures 1 and 2. The energies are listed in Table 4.

Evidently, the CAS(10,8)/6-311G(d,p) optimized geometries of TS1 and TS2 are in reasonable agreement with those obtained using either MP2 or CCSD methods except that the OCO angle of TS2 is too large. The CAS(10,8)/6-311G(d,p) calculated zero-point energies for $O+CH_3COCH_3$, TS1, and TS2 are in good agreement with the ZPEs obtained at the MP2/6-311G(d,p) or CCSD/6-311G(d,p) level.

Because the MCSCF method does not include the important dynamical electron correlations, the barrier heights for TS1 and TS2 were estimated by the multireference configuration interaction with single and double excitations (MRCISD)[34] at the CAS-(10,8)/6-311G(d,p) optimized geometries. Davidson correction, denoted as MRCISD+Q (abbreviated as MR+Q),[35] was employed to estimate the contribution from the higher excitations with the 6-311G(d,p) basis set and the more flexible 6-311++G-(3df,3pd) basis set. The Molpro program[36] was used for the MR+Q calculations.

The energies are listed in Table 4. The coefficients for the HF reference determinants are 0.906 and 0.895 for TS1 and TS2, respectively. Apparently, both involve severe spin contamination. However, the calculated barrier heights for TS1 and TS2 at the MR+Q/6-311++G(3df,3pd) level are in excellent agreement with the values obtained using the coupled-cluster method (e.g., 8.62 vs 8.77 for TS1 and 11.07 vs 10.34 for TS2). Moreover, the barrier TS1 is lower than TS2, which confirms that the direct hydrogen abstraction is the dominant mechanism for the $O(^3P) + CH_3COCH_3$ reaction.

IV. Concluding Remarks

The reaction of $O(^3P)$ with acetone has been investigated theoretically in this work. The structures and energetics of the possible reaction pathways were obtained using high-level ab initio methods. It is revealed that the reaction is dominated by the direct hydrogen-abstraction pathway, forming hydroxyl and acetonyl radicals. The nucleophilic OC addition/elimination mechanism leading to CH_3 and CO_2 has a comparable barrier to the abstraction path. However, it plays a negligible role in the overall reaction because of kinetic factors. Neither the OO addition/elimination nor the S_N2-displacement mechanism is significant in view of their huge barriers along the reaction paths.

The kinetic study confirms that the H-abstraction is the major mechanism for the reaction between $O(^3P)$ and acetone. The rate coefficients show strong non-Arrhenius behavior. It is revealed that the tunneling effect plays a significant role, especially at lower temperatures. Moreover, the reaction has a strong kinetic isotope effect. The present theoretical analysis for the rate coefficients and KIE is in good agreement with the experimental results.

It is worth noting that the agreement between experiment and theory is obtained without any fitting to the experimental values and without any adjustment of parameters. All values used in the kinetic calculations were taken directly from the ab initio quantum chemistry calculations.

Acknowledgment. This work was supported by A Foundation for the Author of National Excellent Doctoral Dissertation of PR China (FANEDD, 200224) and by the Scientific Research Foundation for the Returned Overseas Chinese Scholars, State Education Ministry.

Supporting Information Available: Table S1 lists the MEP data for TS1 and TS2 calculated at the MP2/6-311G(d,p) level and the V_a^G data interpolated at the FCC/CBS level. This material is available free of charge via the Internet at http://pubs.acs.org.

References and Notes

(1) Caralp, F.; Forst, W.; Henon, E.; Bergeata, A.; Bohr, F. *Phys. Chem. Chem. Phys.* **2006**, *8*, 1072 and references therein.
(2) Ayre, C. R.; Madix, R. J. *J. Am. Chem. Soc.* **1995**, *117*, 2301.
(3) Henderson, M. A. *J. Phys. Chem. B* **2004**, *108*, 18932.
(4) Azatyan, V. V.; Gyulbekyan, Zh. Kh.; Nalbandyan, A. B.; Romanovich, L. B. *Arm. Khim. Zh.* **1972**, *25*, 727.
(5) Ambidge, P. F.; Bradley, J. N.; Whytock, D. A. *J. Chem. Soc., Faraday Trans. I* **1976**, *72*, 1870.
(6) Lee, J. H.; Timmons, R. B. *Int. J. Chem. Kinet.* **1977**, *9*, 133.
(7) Faubel, C.; Hoyermann, K.; Wagner, H. Gg. *Z. Phys. Chem. (Neue. Folge*) **1982**, *130*, 1.
(8) Mix, K. H.; Wagner, H. Gg. *Oxid. Commun.* **1983**, *5*, 321.
(9) Roscoe, J. M. *Can. J. Chem.* **1986**, *64*, 1458.
(10) Roscoe, J. M. *Can. J. Chem.* **1988**, *66*, 2325.
(11) Herron, J. T. *J. Phys. Chem. Ref. Data* **1988**, *17*, 967.
(12) Pudzlanowski, A. T.; Loew, G. H. *J. Phys. Chem.* **1983**, *87*, 1081.
(13) Dewar, M. J. S.; Thiel, W. *J. Am. Chem. Soc.* **1977**, *99*, 4899.
(14) Wigner, E. *Z. Phys. Chem. B* **1932**, *19*, 203.
(15) Frisch, M. J.; et al. *Gaussian 03*, revision D.01, Gaussian, Inc.: Pittsburgh, PA, 2003.
(16) Moller, C.; Plesset, M. S. *Phys. Rev.* **1934**, *46*, 618.
(17) Scott, A. P.; Radom, L. *J. Phys. Chem.* **1996**, *100*, 16502.
(18) Gonzalez, C.; Schlegel, H. B. *J. Chem. Phys.* **1989**, *90*, 2154.
(19) Curtiss, L. A.; Redfern, P. C.; Raghavachari, K.; Rassolov, V.; Pople, J. A. *J. Chem. Phys.* **1999**, *110*, 4703.
(20) Purvis, G. D.; Bartlett, R. J. *J. Chem. Phys.* **1982**, *76*, 1910.
(21) Wong, M. W.; Radom, L. *J. Phys. Chem.* **1995**, *99*, 8582.
(22) Halkier, A.; Jorgensen, H. P.; Klopper, W.; Koch, H.; Olsen, J. *Chem. Phys. Lett.* **1999**, *302*, 437.
(23) Huh, S. B.; Lee, J. S. *J. Chem. Phys.* **2003**, *118*, 3035.
(24) He, H.; He, Z.; Cremer, D. *Chem. Phys. Lett.* **2000**, *317*, 535.
(25) Ayala, P. Y.; Schlegel, H. B. *J. Chem. Phys.* **1998**, *108*, 2314.
(26) Johnston, H. S.; Heicklen, J. *J. Phys. Chem.* **1962**, *66*, 532.
(27) Garrett, B. C.; Truhlar, D. G. *J. Phys. Chem.* **1979**, *83*, 2921.
(28) Hu, W.-P.; Liu, Y.-P.; Truhlar, D. G. *J. Chem. Soc., Faraday Trans. 1* **1994**, *90*, 1715.
(29) (a) Atkinson, R.; Baulch, D. L.; Cox, R. A.; Hampson, R. F.; Kerr, J. A.; Rossi, M. J.; Troe, J. *Evaluated Kinetic and Photochemical Data for Atmospheric Chemistry* 2003, Appendix. (b) For CH_3COCH_2 radical, see: Bouchoux, G.; Chamot-Rooke, J.; Leblanc, D.; Mourgues, P.; Sablier, M. *ChemPhysChem* **2001**, *4*, 1439.
(30) Wang, B.; Hou, H.; Gu, Y. *J. Phys. Chem. A* **1999**, *103*, 8021.
(31) Li, X.; Paldus, L. *Int. J. Quantum Chem.* **2000**, *77*, 281.
(32) Krylov, A. *J. Chem. Phys.* **2000**, *113*, 6052.
(33) Hegarty, D.; Robb, M. A. *Mol. Phys.* **1979**, *38*, 1795.
(34) (a) Werner, H. J.; Knowles, P. J. *J. Chem. Phys.* **1988**, *89*, 5803 (1988). (b) Knowles; P. J.; Werner, H. J. *Chem. Phys. Lett.* 1988, **145**, 514.
(35) Langhoff, S. R.; Davidson, E. R. *Int. J. Quantum Chem.* **1974**, *8*, 61.
(36) Werner, H.-J.; Knowles, P. J. MOLPRO, version 2006.1, University College Cardiff Consultants Limited: Cardiff, U.K., 2006.